



ELSEVIER

Contents lists available at [SciVerse ScienceDirect](http://www.sciencedirect.com)

Continental Shelf Research

journal homepage: www.elsevier.com/locate/csr

Research papers

Temporal and spatial variability in fall storm induced sediment resuspension on the Mid-Atlantic Bight

Travis Miles*, Scott M. Glenn, Oscar Schofield

Coastal Ocean Observation Laboratory, Institute of Marine and Coastal Sciences, School of Environmental and Biological Sciences, Rutgers University, New Brunswick, NJ 08901, USA

ARTICLE INFO

Article history:

Received 15 February 2011

Received in revised form

20 July 2012

Accepted 3 August 2012

Keywords:

Sediment resuspension

Coastal oceanography

Turbulence

Autonomous underwater vehicles

Sediment transport

Ocean observing systems

ABSTRACT

Storm-driven sediment resuspension is an episodic process that is an important constraint on sediment transport on continental shelves; unfortunately, the spatial variability of the resuspension and transport processes are poorly quantified using traditional sampling techniques. Using two autonomous underwater gliders, long-range high frequency radar and buoy data, we quantified spatial variability of sediment resuspension and transport in a large fall storm in November of 2009. Wave, wind and current data in conjunction with glider profiles showed that waves and winds mixed the water column, waves initially mobilized the sediment and shear induced turbulence advected sediment throughout the water column. The separation of over 50 km between the two gliders (RU05 and RU21) is used to highlight the spatial variability of sediment resuspension. Both gliders were operating along the 40 m isobath with RU21 located 50 km north of RU05. Sediment resuspension on the New Jersey (NJ) shelf responded to synoptically forced turbulent motions. Currents transported this sediment toward the southwest in the along-shelf axis and onshore on the cross-shelf axis during the peak resuspension on November 13th through November 14th, with resuspension and transport on the southern NJ shelf measured by RU05 approximately twice that of RU21 on the northern MAB. Variability in resuspension profiles between the two gliders was largely a product of smaller mean grain sizes on the southern portion of the NJ shelf. These smaller grain sediment particles had a reduced fall velocity and were more easily retained throughout the water column by turbulent motions.

Published by Elsevier Ltd.

1. Introduction

Coastal storm-driven mixing events are episodic processes (Wiggert et al., 2000; Chang et al., 2001; Zedler et al., 2002) that are important for sediment transport. Despite numerous focused field campaigns on storm induced sediment resuspension (Traykovski et al., 1999; Styles and Glenn, 2002; Traykovski, 2007), the processes dominating the spatial variability of the storm response remains unresolved. The Mid-Atlantic Bight (MAB) is a region impacted by numerous physical forcing processes such as freshwater input from a complex network of rivers and estuaries, wave tidal and inertial fluctuations, variable topographic features such as the Hudson Shelf Valley and the ridge and swale topography (Beardsley and Boicourt, 1981; McBride and Moslow, 1991), the shelf-break jet (Chen and He, 2010) and Gulf Stream eddies near the shelf-break, seasonal wind variability (Gong et al., 2010), the summer cold pool (Lentz, 2008) and powerful winter storms (Beardsley and Boicourt, 1981).

Strong solar insolation drives the formation of the summer cold pool that results in large seasonal variations in the water column stratification between winter and summer seasons (Houghton et al., 1982; Lentz, 2003). This stratification is broken down by extra-tropical cyclones, commonly referred to as fall transition storms (Bigelow 1933, Beardsley and Boicourt, 1981). These storms result in a well-mixed water column in the winter until early spring (Lentz, 2003). The erosion of the stratification is important for the MAB ecosystem as it replenishes nutrients to the surface layer, which stimulates phytoplankton blooms (Xu et al., 2011). The winter phytoplankton bloom is the largest and most predictable biological event on the MAB (Xu et al., 2011). Resuspension of sandy sediments, which are dominant on the middle to outer-shelf of the MAB (Swift and Field, 1981; Amato, 1994; Reid et al., 2005; Goff et al., 2008), is commonly driven by fall transition storms through a combination of waves and currents (Glenn et al., 2008). For example, Styles and Glenn (2005) identified 25 sediment transport events over a 2-year period, with 63% of these events occurring in fall and winter on the MAB.

A combination of waves and currents are responsible for the resuspension and transport of sediment on the continental shelf. Though non-linear interactions between waves and currents

* Corresponding author. Tel.: +1 919 332 2705.

E-mail address: tnmiles@marine.rutgers.edu (T. Miles).

dominate sediment resuspension, seminal work by Grant and Madsen (1979; 1896) provides a qualitative explanation of the independent role each process plays. Wave bottom boundary shear stress can be an order of magnitude larger than current bottom boundary shear stress. From linear-wave theory wave-induced bottom orbital velocities have a similar magnitude to low-frequency currents but operate over a much smaller bottom boundary layer and thus result in an observed order of magnitude larger shear stress. Despite the high shear stress, wave velocities are orbital and therefore result in little net horizontal transport to first order. When sediment is suspended in the water column even relatively minor low-frequency currents are capable of horizontal sediment transport.

Keen and Glenn (1995) and Styles and Glenn (2005) show storm-induced sediment transport is generally aligned along-shelf toward the southwest through modeled and observed bottom currents during Nor'easter storms. Modeled cross-shelf sediment transport was offshore (Keen and Glenn, 1995); however the observed cross-shelf component of the transport was predominantly onshore in Styles and Glenn (2005). These observations are surprising as it might be expected that Nor'easters produce downwelling circulation with offshore bottom transport that is reinforced by the tides; therefore a more complex combination of processes must be important.

Several processes have been hypothesized to account for the onshore transport. Potential factors include topographic interactions that operate over the relatively small (a few kilometers) scale of the ubiquitous ridge and swale topography of the MAB inner shelf (McBride and Moslow, 1991), or over the larger (a few tens of kilometers) scale of the topographic highs associated with ancient river deltas (Glenn et al., 2004). Additionally, Gargett et al. (2004) identified full water column Langmuir cells as a significant driver of sediment resuspension events on the Mid-Atlantic Bight. Keen and Glenn (1995) also identified tides as critical to resuspension and transport modulation, as tidal currents can alternately enhance or reduce the more slowly varying storm driven currents. In their work, the tidal phase was important in determining onshore or offshore veering of the predominant along-shore bottom current. Styles and Glenn (2005) did not observe current veering with tidal phase and saw onshore transport near bottom, though their observations were limited to the 10 m water depth. Given this, the cross-shelf magnitude and direction of sediment transport are still unresolved.

Shipboard observations are likely biased to fair weather conditions as these sampling techniques are limited by the extreme conditions experienced in storms. Benthic tripods are ideally suited to resolve temporal variability effectively during extreme conditions but are expensive to deploy and are not designed to sample horizontal spatial variability. Recent work by Glenn et al. (2008) has demonstrated the potential of using autonomous Slocum gliders for sampling sediment transport events on the continental shelves. This work demonstrated that it is possible to average optical backscatter profiles of a single sensor and obtain results that are consistent with the theoretical understanding of coastal storm induced sediment resuspension. This manuscript builds on these results, using two simultaneously deployed gliders to examine the spatial and temporal variability during a fall transition storm on the MAB.

Hurricane Ida, was a low pressure system that developed into a category two hurricane over the Gulf of Mexico. Ida transitioned into an extratropical cyclone over the southeastern United States on November 10th, 2009. This system, commonly referred to as Nor'Ida, tracked northeastward along the eastern United States coast and into Canada causing extensive damage and coastal flooding. We present data from multiple gliders during Nor'Ida over large along- and cross-shelf spatial scales and incorporate

shelf-wide HF radar surface currents (Roarty et al., 2010) measured with 6 km resolution for the duration of a fall transition storm. Both gliders started from the same location off Tuckerton, New Jersey (Fig. 1) and performed cross-shelf transects offshore. As in Glenn et al. (2008), deviation from flight paths and increases in glider depth-averaged currents indicate storm passage. Glider tracks and depth averaged currents for RU05 and RU21 can be seen in Figs. 2 and 3. RU05 took a brief northeastward turn followed by a long southwestward along-isobath track, which was enhanced by southwestward storm induced currents. RU21 finished its offshore cross-shelf transect and returned to complete an onshore cross-shelf transect, with deviations as a result of southwestward storm induced currents.

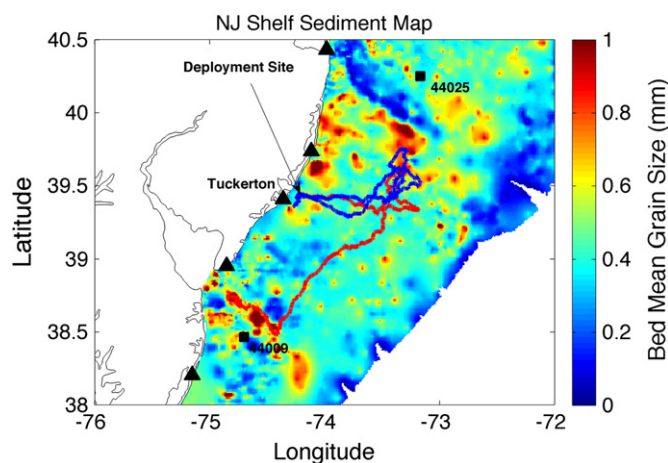


Fig. 1. The study location and 2 km resolution mean grain size map in mm with glider tracks from RU05 (red), RU21 (blue), CODAR locations within the study region (black triangles) and Buoys 44009 and 44025 (black squares). Only CODAR stations in the immediate vicinity are shown, though others contributed to the data. The deployment site for both gliders is off Tuckerton, NJ. RU21 was recovered near the deployment site while RU05 was recovered in the south off of Delaware Bay, near buoy 44009. Details of sediment compilation from the usSEABED program are covered in Goff et al. (2008).

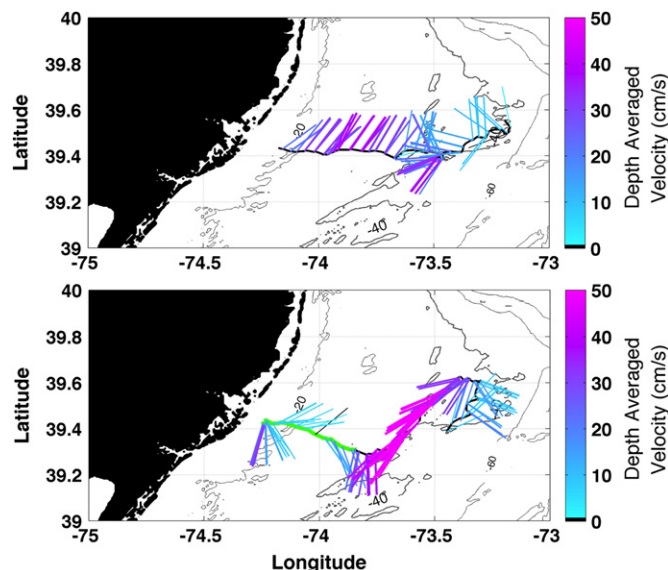


Fig. 2. RU21 depth averaged currents and offshore glider track from 10/31 to 11/05 (Top Panel) and onshore glider track from 11/10 to 11/18 (Bottom Panel). The green line indicates the portion of the transect from 11/15 to 11/18.

2. Materials and methods

This project relied on infrastructure operated by the Mid-Atlantic Regional Association Coastal Ocean Observing System (MARACOOS) that is part of the United States Integrated Ocean Observing System (U.S. IOOS) (Roarty et al., 2010; Schofield et al., 2010a). MARACOOS provides a suite of data collected by satellites, a high frequency CODAR network, and a fleet of Webb Slocum gliders (Glenn and Schofield, 2009). All of the above remote sensing techniques are coupled to a super ensemble of data assimilative numerical ocean models (see below).

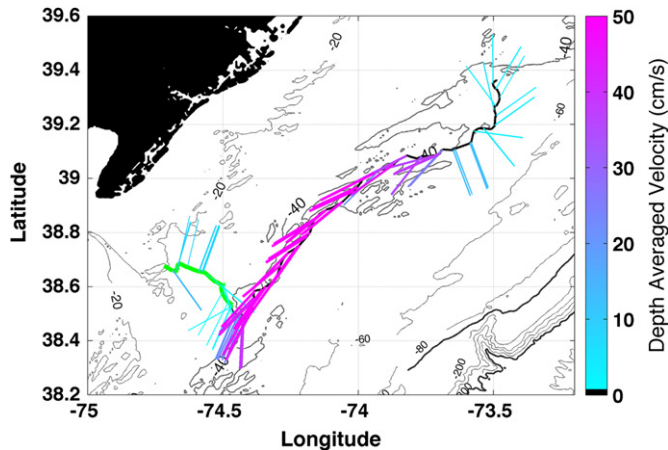


Fig. 3. RU05 glider track and depth-averaged currents between 11/10 and 11/18. The green line indicates the onshore glider track on 11/16 to 11/18.

2.1. Ocean observation dataset

A network of CODAR Ocean Sensors SeaSonde HF Radar systems measures surface currents on the MAB. The CODAR network consisted of 13 5-MHz HF Radar systems located along the northeast of the United States (Fig. 1). The HF Radar uses the Doppler Shift of a radio signal backscattered off the ocean surface to measure the component of the flow in the direction of the antenna (Barrick, 1971a, 1971b; Teague, 1971). Descriptions of the CODAR data and its shelf-wide applications are outlined in Dzwonkowski et al. (2009b) and Gong et al. (2010). The network provides surface current observations at the estimated equivalent depth of 2.4 m (Stewart and Joy, 1974). To minimize the geometric uncertainty in the radials we used the recommended threshold for the Geometric Dilution of Precision (GDOP) (Chapman and Graber, 1997) value of 1.5 or less to identify the vectors with acceptable GDOP (Dzwonkowski et al., 2009a). This value is chosen based on current comparison studies using CODAR and ship-mounted Acoustic Doppler Current Profilers (Kohut et al., 2006) and drifters (Ohlmann et al., 2007). The spatial resolution of the final total vector current maps is 6 km with a typical cross-shelf range of 150 km.

Sediment mean grain size is determined by taking a regional subsample of a 2 km resolution interpolated sediment map developed by Goff et al. (2008) from data compiled as part of the usSEABED project (<http://walrus.wr.usgs.gov/usseabed/>). We convert phi units into mm grain size as the sandy sediment only varies over two phi units (Fig. 1).

Oceanographic data from NOAA NDBC buoys 44009 and 44025 were used in this effort (Fig. 1). The moorings provided data on atmospheric pressure, wind speed/direction, wave-height, period and direction (Fig. 4).

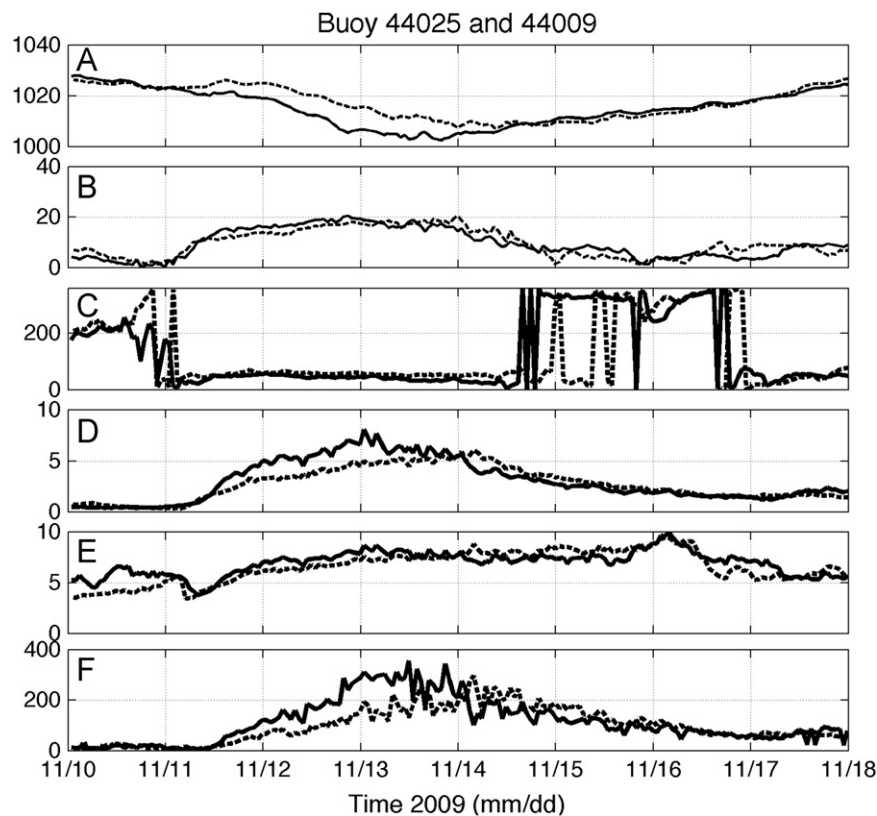


Fig. 4. Buoy 44009 (solid line) and 44025 (dashed line) (A) sea-level-pressure, (B) 5 m wind speed, (C) wind direction (D) wave height (E) wave period and (F) bottom orbital velocities for 11/10 to 11/18. Wave induced bottom orbital velocities were calculated from linear wave theory as in Glenn et al. (2008).

Slocum gliders are an autonomous underwater scientific platform (Davis et al. 2003; Schofield et al., 2007) manufactured by the Teledyne Webb Research Corporation. They are 1.8-m long, torpedo-shaped, buoyancy-driven vehicles with wings that enable them to maneuver through the ocean at a forward speed of $20\text{--}30\text{ cm s}^{-1}$ in a sawtooth-shaped gliding trajectory. A full description of our scientific operation of the Slocum gliders can be found in Schofield et al. (2007). Each Slocum glider has a payload bay that houses a SeaBird conductivity–temperature–depth sensor and includes space for a range of additional sensors. The glider acquires its global positioning system (GPS) location every time it surfaces, a programmable interval that was set to 3 h for the purposes of this study. By dead reckoning along a compass bearing while flying underwater, estimates of depth averaged current can be calculated based on the difference between the glider's expected surfacing location and the actual new GPS position. Depth averaged current measurements obtained in this manner have been validated against stationary Acoustic Doppler Current Profiler data (Davis et al. 2003). These physical measurements are complemented with several bio-optical sensors (Glenn and Schofield, 2009).

Two Webb Slocum gliders were deployed prior to November 1, 2009 and operated for two weeks. During that period the gliders traversed 1673 km underwater collecting 23,332 vertical profiles (Fig. 1). The gliders were outfitted with WetLabs Inc. EcoPucks, which provide measurements of optical backscatter, chlorophyll fluorescence and colored dissolved organic fluorescence. The

EcoPucks measure optical backscatter at 440 (b_b470) and 660 (b_b660) nm. Optical backscatter, to first order, is used to measure the relative concentration of particulate matter (Roesler and Boss, 2008). A growing body of work indicates that optical backscatter is not only a function of particle concentration but also sediment characteristics such as refractive index, size, shape and particle composition (Twardowski et al., 2001; Boss et al., 2004). While we do not characterize sediment in great detail during the measured resuspension events, we use changes in backscatter ratios to indicate a change in character of suspended particles.

2.2. Adaptive sampling

To coordinate the numerous observed and forecast model data streams, we were able to utilize a novel cyberinfrastructure (CI) tool set being developed as part of the Ocean Observing Initiative (OOI). The software was used to coordinate sampling using multi-model forecasts to optimize glider missions (Schofield et al., 2010b). In brief, numerical model ocean forecasts allowed the simulation of future *in situ* glider trajectories. This guidance could be used by the team to optimize sampling based on the science needs. This provided scientists with a guide to determine whether desired target areas could be reached by Webb Slocum gliders in a predicted current field. Thus the CI software could deliver the community science needs back to the *in situ* observation network in a timely manner. Field operations were coordinated through a

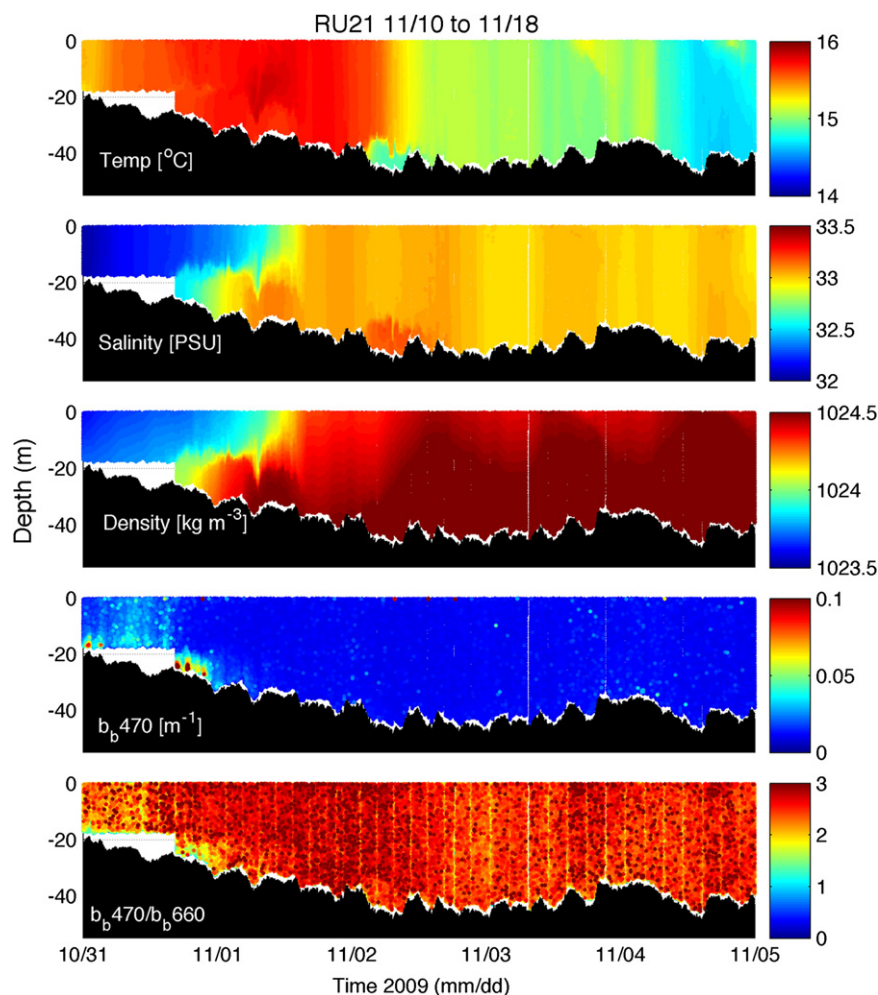


Fig. 5. RU21 Pre-storm cross sections of temperature, salinity, density, b_b470 and the ratio of b_b470/b_b660 .

web portal (<http://ouroecean.jpl.nasa.gov/CI>) that provided an access point for real-time observational data and model forecasts.

3. Results

3.1. Pre-storm hydrography

Pre-storm conditions were typical for fall on the MAB with predominantly vertical isotherms and a cross-shelf temperature gradient. RU21, on its offshore transect (Fig. 2) between October 31st and November 5th, showed a near-shore water mass that was approximately 1 kg m^{-3} lighter than offshore waters (Fig. 5). This lower density coastal water was largely due to the variability in salinity. Additionally, there was a warm core of water centered at 15 m depth, on the 35 m isobath, which contributed to the regional vertical and horizontal density gradients. This glider data shows that New Jersey shelf waters were generally colder, saltier and denser in the offshore direction. B_b470 was low ($< 0.005 \text{ m}^{-1}$) for the majority of the offshore pre-storm transect. There is a small region of elevated backscatter near-shore located below the pycnocline. RU21 was not programmed to dive below 20 m until after it reached the 25 m isobath so the optical backscatter at the bottom in the near-shore region was not completely sampled. Pre-storm water column b_b470 to b_b660 ratios were high (~ 3) relative to storm signatures (see below). There was a short period of elevated currents toward the northeast in the coastal region (Fig. 2). Prior to the storm both the gliders and CODAR (Figs. 2, 3, 6) showed variable currents between 5 and 40 cm s^{-1} along the coast of New Jersey, with daily averaged currents immediately prior to the storm event somewhat higher than the climatological mean of 5 cm s^{-1} (Beardsley and Boicourt, 1981).

3.2. Storm data

Buoy 44009, off of Delaware Bay, and 44025, off Long Island are separated by approximately 230 km with 44009 encountering Nor'Ida first (Fig. 4). As the storm entered the MAB region from the southwest, pressure fell from above 1020 mbar at both buoys to a minimum of 1002 mbar on November 13th at 2000 Greenwich Mean Time (GMT) at 44009 and a minimum of 1007 mbar on November 13th at 2350 GMT at 44025 (Fig. 4A). Winds at both locations began to increase at 0000 GMT on November 11th, but peak winds at 44025 lagged 44009 by 28 h with slightly lower magnitude until they reached a maximum of 20.5 ms^{-1} at 23:50 GMT on November 13th (Fig. 4B). Prior to November 11th

wind direction was variable. Between November 11th and late on the 15th, wind direction at both buoys was from the northeast (Fig. 4C). Wave-heights began to build after a few hours of rising winds at both locations (Fig. 4D). Wave heights reached over 8 m at 0050 GMT on November 13th at 44009 and over 6 m at 0350 GMT on the 14th at 44025. Wave spectral periods were between 7 and 9 s for the duration of the storm at both locations and continued to increase after storm passage, eventually peaking at $\sim 10 \text{ s}$ on the morning of November 16th (Fig. 4E). Maximum wave bottom orbital velocities were calculated from buoy data using linear wave theory as described by Glenn et al. (2008). Wave bottom orbital velocity estimates peaked at 2.4 m s^{-1} and 1.8 m s^{-1} at buoy 44009 and 44025 respectively (Fig. 4F), significantly higher than glider depth-averaged and CODAR surface currents (Figs. 2, 5, 8).

CODAR daily averaged currents (Fig. 6) were toward the southwest on November 11th and reached 30 cm s^{-1} on the central and southern MAB with values offshore nearing 50 cm s^{-1} . CODAR daily averaged surface currents peaked in excess of 50 cm s^{-1} shelf-wide on the central and southern MAB on the 13th. There was a low velocity region on the northwestern MAB near the Hudson River outflow. Over the two days following peak values, shelf-wide currents decreased back to near pre-storm values, below $\sim 15 \text{ cm s}^{-1}$.

3.3. RU21 northern glider storm variability

As Nor'Ida approached the New Jersey shelf, RU21 turned onshore and attempted to retrace the path of its offshore transect (Fig. 2). Initially it flew southwestward along the 40 m isobath until it turned onshore on the 15th. Cross-sections of glider measurements (Fig. 7) show that during its southwestward transect RU21 initially measured vertically uniform temperatures of 15°C , salinity of 33 PSU, density near 1024.6 kg m^{-3} , optical backscatter at $b_b470 \text{ nm}$ was near 0 m^{-1} and the ratio of b_b470 to b_b660 was ~ 3 . Downcast vertical glider velocities were uniform at $\sim 0.3 \text{ m s}^{-1}$. Vertical glider velocities were calculated by the change in measured pressure over time and we used them to serve as a proxy for vertical water velocities. In uniform water masses with no external turbulent forcing and the glider on a new constant glide slope, vertical velocities should have also remained approximately constant except when the glider was inflecting near-bottom or near-surface.

As winds, waves and currents increased beginning on the 11th, there was a distinct water column response. First, glider vertical velocities began to undergo high-frequency variability of ~ 0.1 to

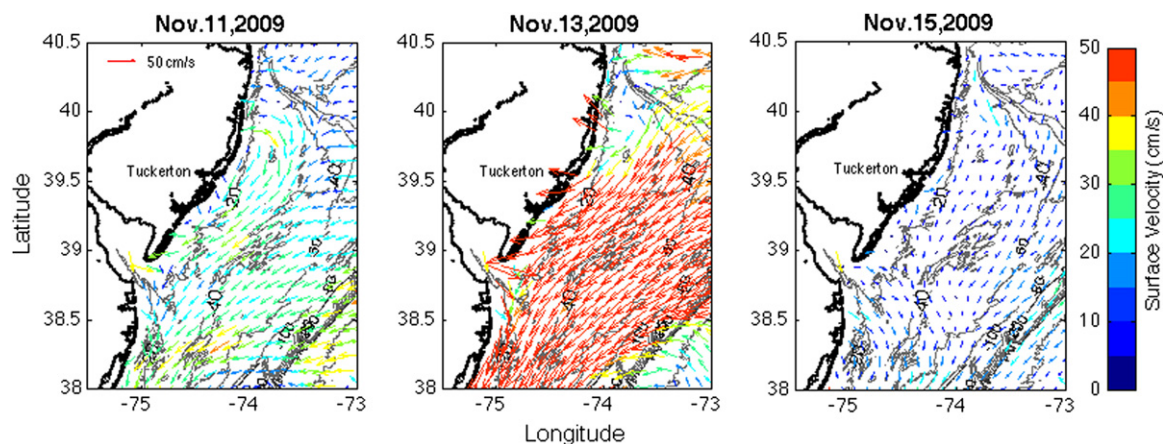


Fig. 6. Daily averaged CODAR surface currents for the New Jersey shelf for November 11th 13th and the 15th. Black contours represent bottom topography in units of meters.

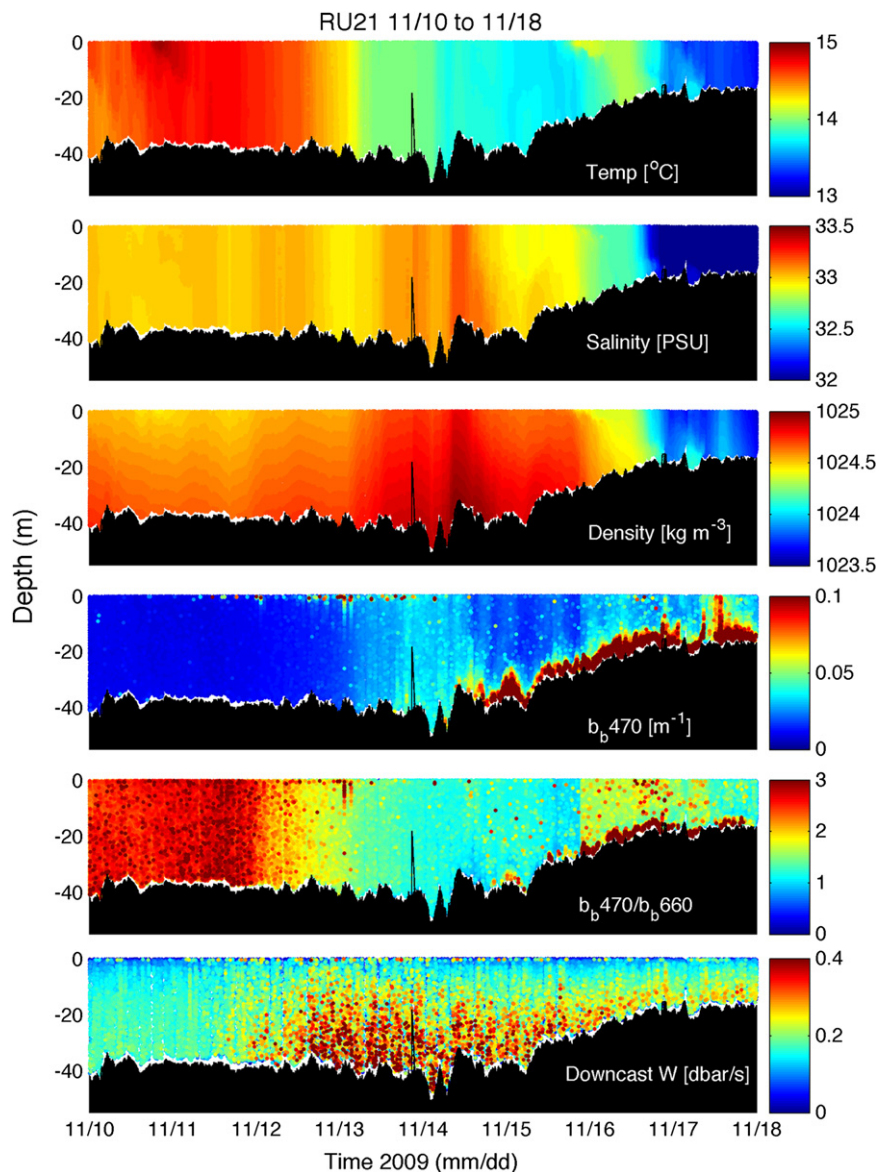


Fig. 7. RU21 during and post-storm cross-sections of temperature, salinity, density, b_b470 , b_b470/b_b660 and downcast glider vertical velocities.

0.2 m s^{-1} through the entire water column. These vertical velocity variations persisted through the 14th until they were restricted to a bottom layer and eventually relaxed after the 16th. As the magnitude of vertical velocities increased, temperatures cooled to 14°C , salinity was elevated above 33 PSU and 1025 kg m^{-3} density water was raised to the surface. Values of b_b470 of $\sim 0.05 \text{ m}^{-1}$ were evident throughout the water column on the 13th. The enhanced particle load remained suspended until the afternoon of the 14th. Optical backscatter spectral ratios changed from 3 to 1 as Nor'lda impacted the region, reflecting a flattening of the backscatter spectra consistent with changes in either particle type and/or particle size in the water-column (Boss et al., 2004).

Previous studies have clearly defined the Rouse profile above the wave boundary layer (Glenn et al., 2008; Styles and Glenn, 2000; Glenn and Grant, 1987) as

$$C(z) = C(z_r) \left[\frac{z}{z_r} \right]^{[-\gamma w_f / \kappa u_*]} \quad (1)$$

where $C(z)$ is the concentration profile varying with depth z , $C(z_r)$ is the concentration at the reference height z_r , γ is a constant ratio of eddy diffusivities between momentum and mass, κ is von Karman's constant and u_* is friction velocity. Assuming constant γ (Glenn and Grant, 1987), the slope of $\ln(C(z)/C(z_r))$ to $\ln(z/z_r)$ is proportional to the ratio of the fall velocity, the tendency of sediment to fall out of the water column, to the friction velocity representing the turbulent shear that acts to keep sediment suspended in the water column, or w_f/u_* . In order to identify this ratio, we use optical backscatter as a proxy for sediment concentration similar to Glenn et al. (2008). Optical backscatter profiles were interpolated every 1 m in a reference frame measured from the bottom and averaged over three-hours. These three-hour profiles were then normalized using the backscatter observed at a 3.5 m reference height and plotted as the $\ln(z/z_r)$ versus $\ln(b_b(z)/b_b(z_r))$. The 3.5 m reference height ensures all profiles in each three-hour segment have data at this height and above. Normalized backscatter profiles from RU21 (Fig. 8) demonstrated Rouse-like character from the 14th at 04:24 GMT until the

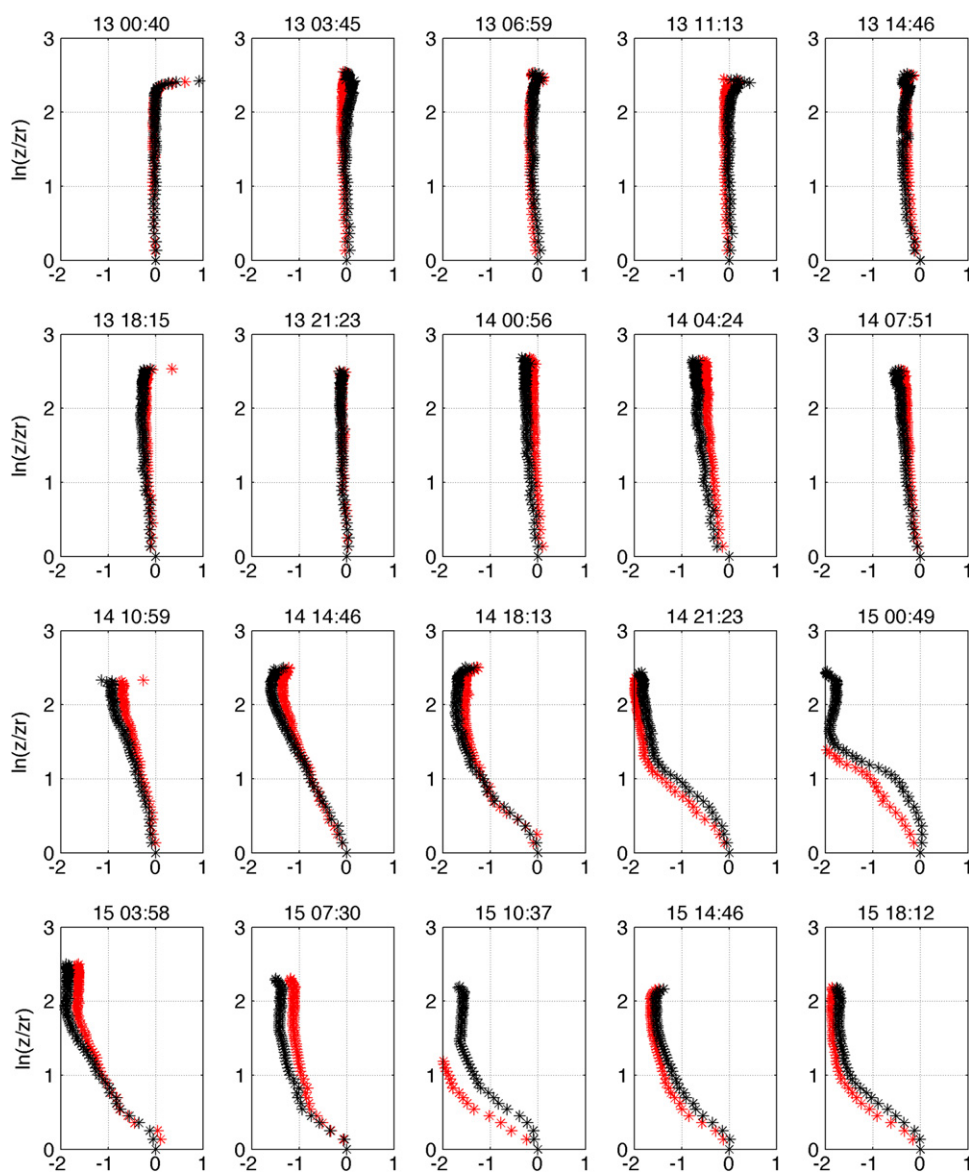


Fig. 8. RU21 log-normalized profiles of optical backscatter at b_{b470} (red) and b_{b660} (black). Y-axis is the natural logarithm of depth divided by z_r , a reference depth of 3.5 m. The X-axis is the natural logarithm of optical backscatter, b_b , divided by the optical backscatter at the reference depth b_r or $\ln(b/b_r)$. Titles are timestamps of November dd HH:MM.

14th at 21:23 GMT. High near-surface values in rough seas are likely due to bubbles being entrained by breaking waves. Terrill et al. (2001) has observed optical backscatter values of over 0.016 m^{-1} inside bubble clouds.

On November 15th, at approximately 06:00 GMT, RU21 turned onshore and left the 40 m isobath, indicated by the green section of Fig. 2b. As the glider entered the shallow coastal region, temperature, salinity and density remained well-mixed in the vertical while there were horizontal gradients of $\sim 1^\circ \text{C}$, $\sim 1.5 \text{ PSU}$ and $\sim 1.5 \text{ kg m}^{-3}$ respectively (Fig. 7). On the 15th to the 18th a layer of high b_{b470} , over 0.1 m^{-1} , was apparent, elevated to 10–15 m off the bottom (Fig. 7). Profiles (Fig. 8) show a layer restricted below $\ln(z/z_r) = 1.5$, roughly equivalent to 15 m. The lower layer persists through the remainder of the deployment. Though winds and currents were reduced, wave-heights, wave-periods and bottom orbital velocities remained significantly elevated (Fig. 4). Glider measured vertical velocity variability remained elevated in the near-bottom layer through the 16th (Fig. 7).

3.4. RU05 southern glider storm variability

Between the 10th and 16th of November, RU05 was on a southwestward track along the 40 m isobath (Fig. 3). RU05 turned onshore toward the mouth of the Delaware River on the 16th through the 18th. RU05 cross-sections (Fig. 9) show that on November 10th the water column was initially stratified with relatively cool ($\sim 14^\circ \text{C}$) and salty ($\sim 33.5 \text{ PSU}$) bottom water, likely a remnant of the summer cold pool. Cross-sections show that dense bottom water was advected through the lower half of the water column late on the 10th into the 11th. There were periodic bulges of weakly stratified water ($0.6\text{--}0.2 \text{ kg m}^{-3}$), which grew progressively weaker until the water column was vertically well mixed on the 16th. Similar to RU21, b_{b470} was low initially and spectral ratios of b_{b470} to b_{b660} were ~ 3 . Vertical velocities were initially constant at $\sim 0.3 \text{ m s}^{-1}$ and variations of $0.1\text{--}0.2 \text{ m s}^{-1}$ were apparent during elevated wind, waves and currents. A consistent background b_{b470} value of 0.05 m^{-1} is apparent throughout the water column, and near-bottom values

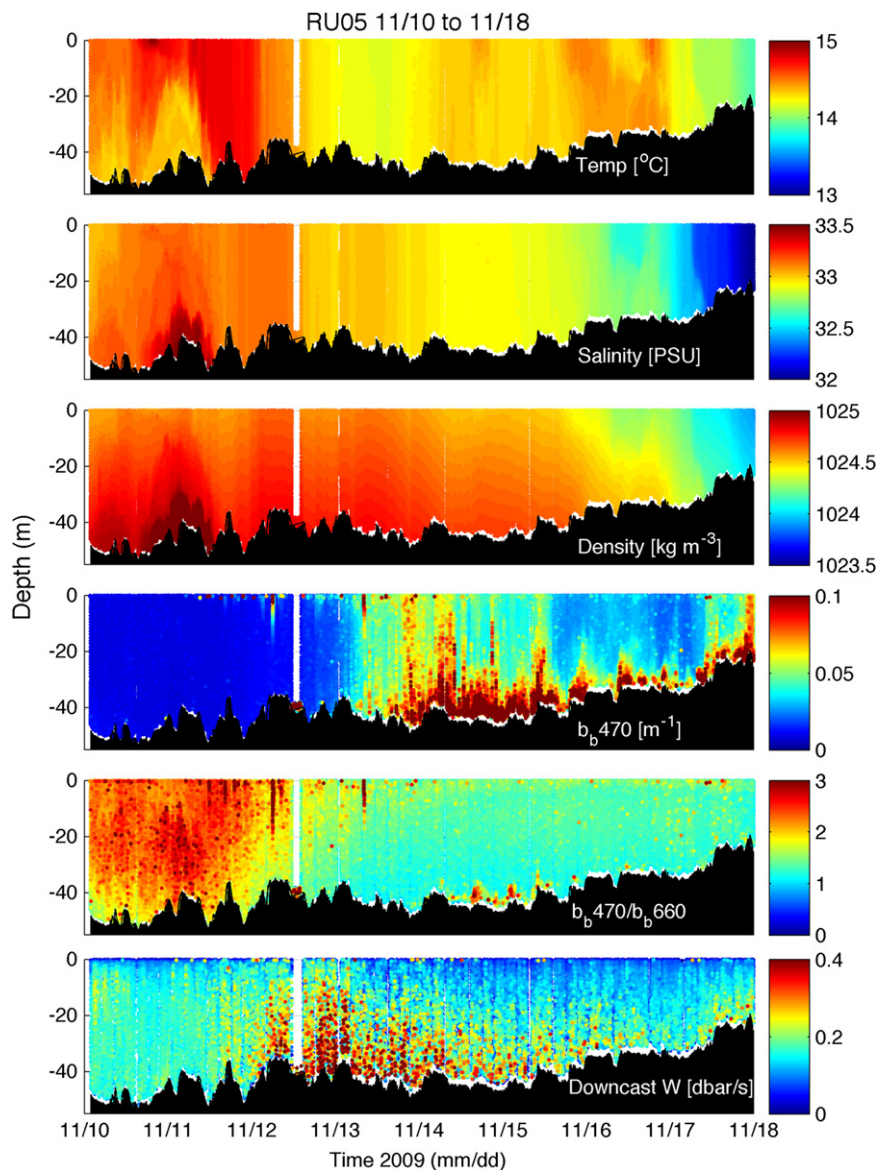


Fig. 9. RU05 cross-section of temperature, salinity, density, b_b470 , b_b470/b_b660 and downcast glider vertical velocities.

are near 0.1 m^{-1} until RU05 turns onshore on the 16th. Unlike RU21, there were periodic full water column resuspension events with b_b470 of 0.1 m^{-1} that occur on time-scales less than a day. Similar to RU21, ratios of b_b470 to b_b660 dropped, which indicated changes in either particle type and/or particle size (Boss et al., 2004). Regardless of the periodicity seen in b_b470 cross-sections, the ratios are constant and ~ 1 after the resuspension event was initiated.

RU05 profiles of optical backscatter (Fig. 10) were calculated in the same manner as for RU21 and for the same duration, from November 13th through the 15th. Reference depth normalized profiles were near 0 until 21:02 GMT on the 13th when the profiles became Rouse-like approximately eight hours earlier than the northern glider, RU21. RU05 then turned onshore toward the Delaware River mouth on the 16th to the 18th (indicated by green in Fig. 3), vertical velocities, winds and currents were reduced, while wave-height, period and orbital velocities remained elevated relative to pre-storm conditions.

3.5. Sediment transport

Three-hourly averaged CODAR surface velocities were compared with approximately three-hourly depth-averaged glider currents (Fig. 11). CODAR velocities are averaged in a 10 km radius of each glider surfacing latitude and longitude. There is a minor temporal and spatial mismatch between glider depth-averaged and CODAR currents as glider currents are averaged over a three-hour subsurface transit obtained by dead reckoning along a compass bearing and comparing the expected glider surfacing location with the actual surfacing location. Depth-averaged currents obtained in this manner have been validated against traditional current measurements from stationary ADCPs (Davis et al., 2003) While we could not obtain any subsurface current structure information directly, by comparing depth-averaged and surface currents, we can make some inferences about how subsurface currents change during the storm.

RU21 and RU05 depth-averaged along-shelf currents both showed similar results when compared with CODAR currents

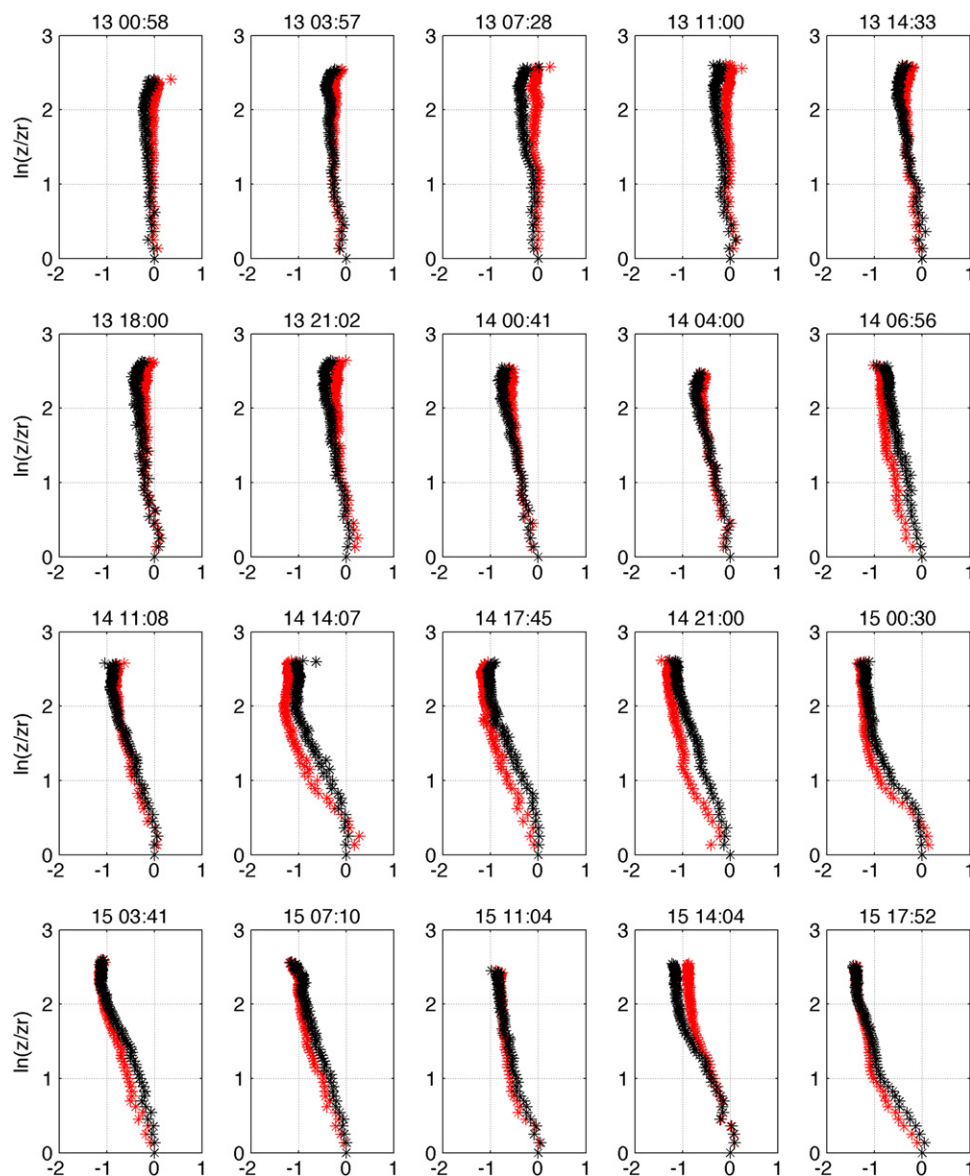


Fig. 10. RU05 log-normalized profiles of b_{b470} (red) and b_{b660} (black). Y-axis is the natural logarithm of depth divided by z_r , a reference depth of 3.5 m. The X-axis is the natural logarithm of optical backscatter, b_b , divided by the optical backscatter at the reference depth b_r or $\ln(b/b_r)$. Titles are timestamps of November dd HH:MM.

for the duration of each glider deployment. The storm event is easily identifiable in both gliders, which were approximately along the 40 m isobath, between the 10th and 15th, with onshore currents up to 40 cm s^{-1} and alongshore currents toward the southwest of up to 80 cm s^{-1} . Correlation coefficients calculated between glider and CODAR currents for the entire deployment showed a weak correlation in cross-shelf currents of 0.30 for RU05 and 0.33 for RU21. Correlation coefficients in the along-shelf direction were much greater, with values of 0.81 for RU05 and 0.77 for RU21. Correlation coefficients of CODAR and glider comparisons limited to during and after the storm, from the 10th to the 18th, showed that the cross-shelf components increased to 0.44 for RU05 and 0.5 for RU21 and the along-shelf components remained essentially the same at 0.81 for RU05 and 0.84 for RU21. The weak cross-shelf correlation coefficients suggest that deeper currents were initially weaker and not necessarily in the same direction as surface currents. Increased correlation during and after the storm suggest that subsurface currents in the cross-shelf direction either increased in magnitude or aligned more closely with surface currents.

In order to estimate sediment transport magnitude and direction, a time-series of integrated b_{b470} was calculated by integrating over depth and segment b_{b470} during the RU05 and RU21 deployments and then (Fig. 12). These depth and time integrated plots show elevated values of backscatter that initiated on the 13th and remained elevated through the duration of the storm until the 16th with the southern glider, RU05, showing much larger values during the storm. The northern glider, RU21, had a second peak after the storm, which was approximately double the size of the storm-induced values. Estimated transport was calculated by multiplying the integrated backscatter by the along- and cross-shelf depth-averaged currents reported by the gliders (Fig. 12). Prior to the storm, low sediment concentrations and low currents result in transport near 0 s^{-1} . During the resuspension event, sediment was transported toward the southwest in the along-shelf (Fig. 12) direction for both RU05 and RU21. RU05 showed approximately twice the along-shelf sediment transport as RU21 during the storm. RU05 and RU21 cross-shelf transport was approximately half of the along-shelf transport and in the onshore direction during the storm. Following the storm RU05

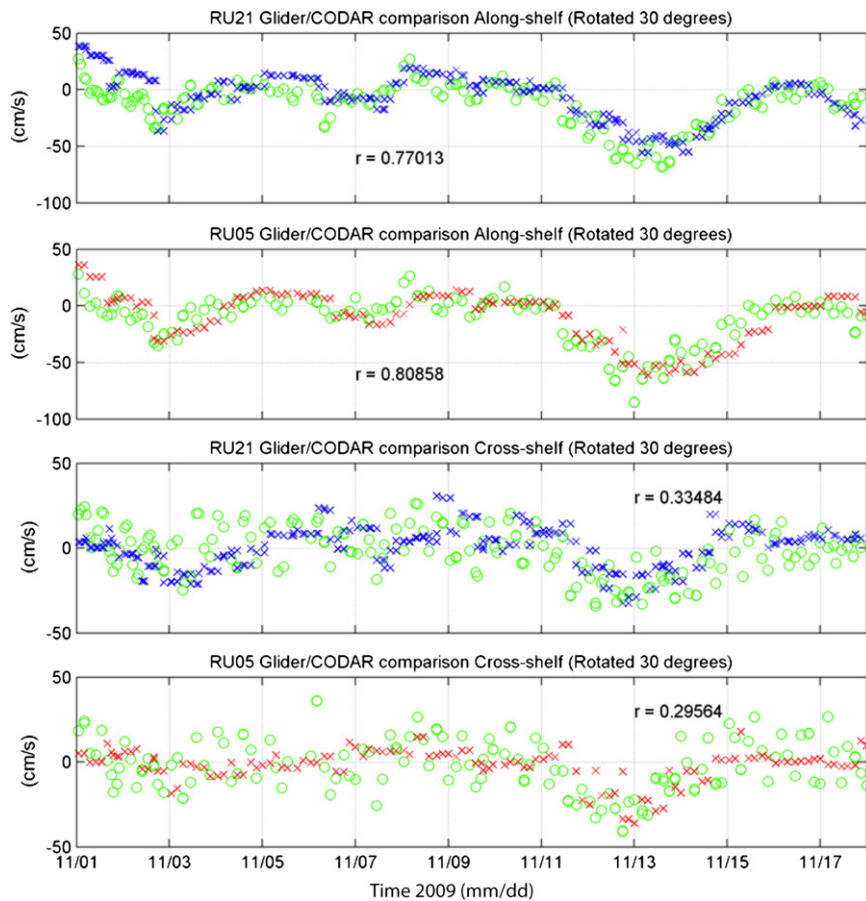


Fig. 11. Along-shelf currents for RU21 and RU05 (Top two panels) and cross-shelf currents for RU21 and RU05 (Bottom two panels) depth averaged glider currents (x 's) and along-track 3-hourly averaged CODAR surface currents (o 's) rotated clockwise 30 degrees to be in the cross- and along-shelf directions with positive along-shelf currents to the northeast and positive cross-shelf currents to the southeast. Correlation coefficients for the full time-period are displayed as r .

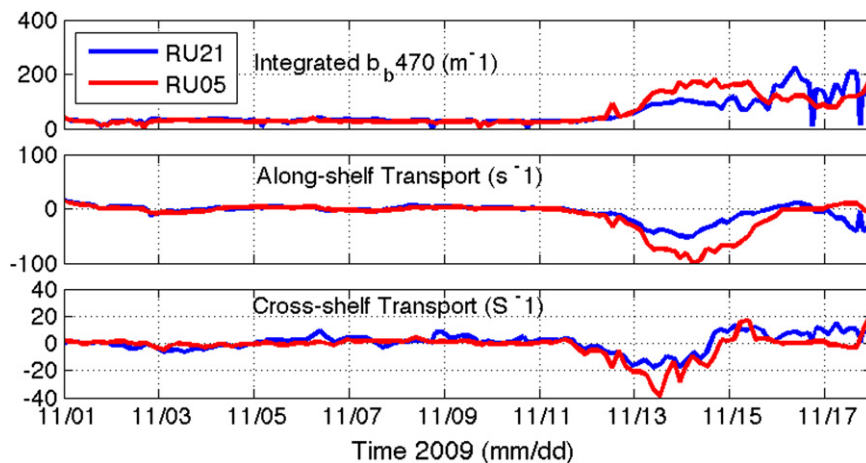


Fig. 12. Time-series of the (blue) RU21 and (red) RU05 (top) three-hour integrated b_{470} (m^{-1}) and estimated transport in the (middle) along- and (bottom) cross-shelf directions. Positive values indicate northeastward transport for along-shelf and southeastward transport for cross-shelf transport. Estimated transport is calculated by multiplying depth-averaged glider currents by integrated optical backscatter at b_{470} .

transport was reduced to near $0 s^{-1}$ when currents and integrated backscatter were both reduced (Fig. 12). RU21 transport shifted to the offshore direction as high b_{470} still remained in the water column (Fig. 12) and current velocities were reduced (Fig. 11) as it approached the coast.

4. Discussion

While many studies have focused on sediment resuspension at a single point on the MAB shelf (Traykovski et al., 1999; Agrawal and Pottsmith, 2000; Harris et al., 2003; Agrawal,

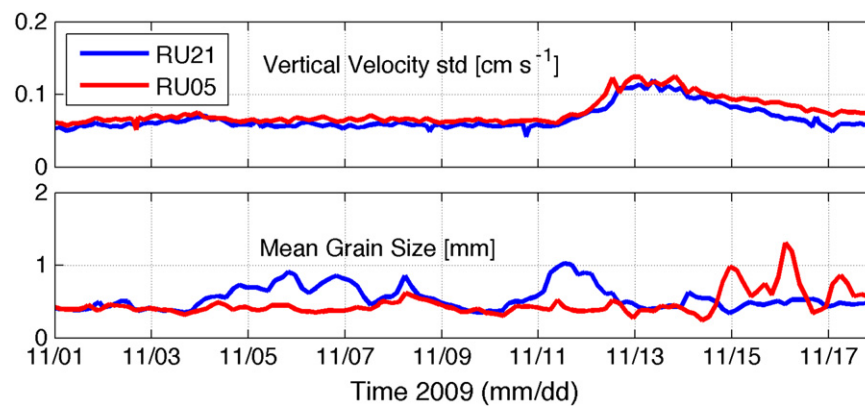


Fig. 13. Time-series of the (blue) RU21 and (red) RU05 (top) three-hour segment standard deviation of vertical velocity (cm s^{-1}) and (bottom) mean bed grain-size from Fig. 1 interpolated to the along-track glider positions.

2005; Traykovski, 2007; Cacchione et al., 2008) few observational studies have focused on the shelf-wide spatial variability of these processes. We were fortunate to have several gliders deployed to assess the spatial variability of sediment resuspension on the MAB during the Nor'Ida fall transition storm (Schofield et al., 2010b). The two gliders equipped with optical sensors, separated by ~ 50 km at the onset of storm conditions, documented the initiation of sediment resuspension through the increases in optical backscatter. Just like the two gliders, buoys 44009 and 44025 (separated by 230 km) showed similar characteristics, with a 1-day lag in peak values, through the initiation of elevated storm winds and waves. Despite the separation distances, along-shelf transport toward the southwest was a ubiquitous feature of both glider deployments with a lag in resuspension of approximately eight hours. With a separation distance of ~ 50 km this lag is on the same order as the lag seen in peak storm conditions at buoys 44025 and 44009. Peak sediment transport was associated with a combination of a maximum in suspended sediment concentration and high relative along-shelf southwestward currents. The nearly coincident maximum in sediment transport suggests that along-shelf transport is a common feature of the entire NJ shelf and MAB and is consistent with previous modeling studies (e.g. Keen and Glenn, 1995). The event duration is longer than the temporal lag between the southern and northern gliders so the large-scale storm effectively forces the shelf as a whole and there is little spatial variability in the timing of resuspension and transport as a result of storm passage.

While resuspension and transport occurred with an approximately eight hour lag, the strength of resuspension and transport varied by as much as a factor of two in the along-shelf direction, with higher transport associated with RU05 located on the southern NJ shelf. The major difference in sediment resuspension, and consequent transport, was related to the numerous discrete resuspension events that resulted in high sediment concentrations up into the water-column during the storm. The difference in the scale and frequency of resuspension events over spatial scales much smaller than the storm event points out the importance of local processes, which affect the magnitude of sediment resuspension and transport. Previous work by Styles and Glenn (2005); Keen and Glenn (1995); Gargett et al. (2004) have highlighted tidal forcing, topographic variations and Langmuir cells as potential processes affecting sediment resuspension and transport on time-periods shorter than a day. For both gliders, vertical velocity variability appeared random rather than spatially banded (Figs. 7 and 9), indicating that Langmuir cells were not likely the cause of the suspended sediment spatial heterogeneity. RU21 and RU05 were both flying approximately southwestward along the 40 m isobath during elevated winds, currents and waves

therefore topography was essentially constant during the resuspension event (Figs. 7 and 9). RU21 did not experience fluctuations of sediment resuspension or transport on time-scales shorter than a day after the resuspension event was initiated, thus tidal forcing was not likely a dominant modulation process as in Keen and Glenn (1995). The scale of tidal forcing on the shelf is also much larger than the separation distance between the gliders; therefore variability seen in RU05 on shorter time-scales is likely not related to tidal fluctuations.

Glenn et al. (2008) suggested that in the absence of stratification, turbulence in the combined wind-driven surface layer and wave-enhanced bottom boundary layer is responsible for sediment resuspension upward through the water column, but observations were sparse. During the Nor'Ida storm there was a distinct change in vertical glider velocities, which serves as evidence of turbulence in the water column. The standard deviation of each three-hour glider segment for RU21 and RU05 vertical velocities show a distinct increase in vertical velocity variability beginning on the morning of the 12th and persisting through the 16th (Fig. 12). These fluctuations in the glider's vertical velocity serve as an estimate of the turbulent motions due to high storm-induced current-shear, similar to neutrally buoyant lagrangian floats used in Harcourt and D'Asaro (2010). Vertical velocity standard deviation values were approximately the same for RU05 and RU21. Uniform vertical velocity standard deviations suggest that the vertical component of turbulence was similar between the northern and southern portions of the NJ shelf, which is consistent with the scale of the storm and the uniform winds, waves and currents.

With little variability in turbulent vertical velocities between gliders, the differences in bed grain size likely play a major role in modulating the magnitude of resuspension by storm-induced turbulence. In order to assess the importance of local variability in grain size we interpolate mapped values (Goff et al., 2008; Reid et al., 2005) plotted in Fig. 1 to glider latitude and longitude. The resulting time-series (Fig. 13) shows mean grain size below the gliders throughout the deployment. The time-series shows mean grain sizes ranged from ~ 0.3 to ~ 1.4 mm with largest grain sizes seen by RU05 after storm passage, when it turned into the mouth of the Delaware. RU21 passed over a region of over 1 mm grain sizes between the 11th and 13th, after storm initiation but prior to peak conditions. The map in Fig. 1 shows a patch of coarse sediment along the northern portion of the NJ shelf where RU21 was flying and relatively smaller grain sizes in the along-shelf region where RU05 sampled, prior to turning in toward Delaware Bay. During the resuspension events on the 13th through the 15th, RU05 was located over a patch of sand with a mean grain size of 0.3 mm–0.4 mm (Fig. 13) before flying through a region

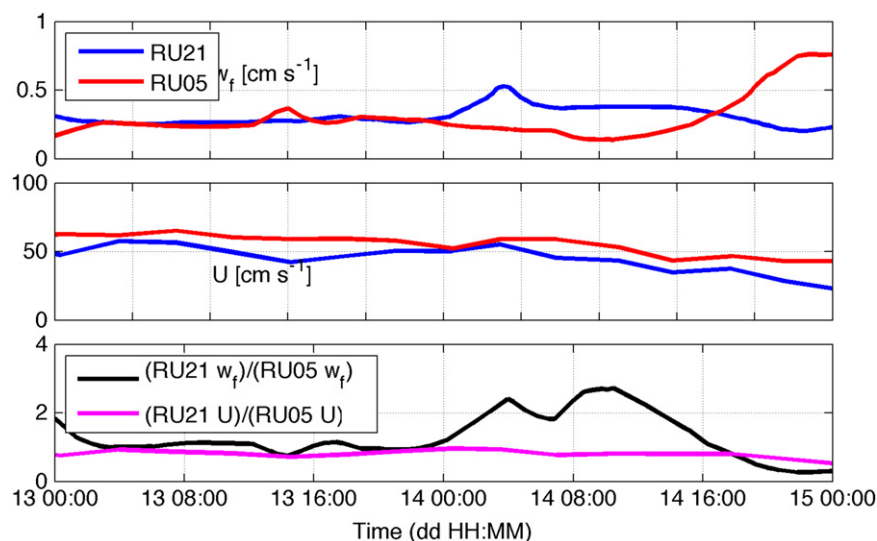


Fig. 14. Time-series of (top) estimated fall velocities for (blue) RU21 and (red) RU05, (middle) magnitude of depth-averaged currents for (blue) RU21 and (red) RU05, and (bottom) the ratio of (black) RU21 to RU05 fall velocities and (magenta) depth-averaged currents, all during the resuspension event.

with mean grain size of over 0.8 mm on the 15th. Conversely, RU21 was in a region with mean grain sizes from 0.4 mm to 0.6 mm on the 13th through 14th. On the 15th RU21 entered a region of reduced mean grain size of $\sim 0.3 \text{ m}^{-1}$.

A study by Agrawal and Pottsmith (2000) as part of the LEO-15 project, which took place within a few kilometers of the deployment location of RU05 and RU21, developed a local model for the fall velocity: $w_{f,n} = 0.45 \times 10^{-3} a_n^{1.2}$ where a_n is the radius in microns and w_f is the settling velocity in cm s^{-1} . As mentioned previously fall velocity is essentially the tendency of sediment to fall out of concentration and u_* is the tendency for particles to remain in suspension. Following the above equation we calculate fall velocities for the sediment grain sizes mapped below the glider during the resuspension event on the 13th through 15th (Fig. 14). Fall velocities are initially greater for RU21 at the peak of the storm, and initiation of the resuspension event at midnight on November 13th. As the gliders progress fall velocities are approximately equal for RU21 and RU05 until the 14th when RU21 fall velocities increase and RU05 fall velocities decrease. While we use the standard deviation of glider vertical velocities as a relative approximation of the timing of turbulent motions, these values are not sufficient to directly substitute for values of u_* . Lentz et al. (1999) uses depth-averaged velocities to estimate bottom stress τ_b . If we follow this model and subsequently calculate a depth-averaged representative friction velocity then we would see u_* values proportional to glider velocities. A time-series of depth-averaged velocities during the storm event are shown in Fig. 14. RU05 depth-averaged velocities are $\sim 5\text{--}10 \text{ cm/s}$ greater than RU21 through the 13th and are approximately equal on the 14th. As our depth-averaged velocities are only proportional to friction velocity we cannot calculate a direct ratio of w_f/u_* .

For comparison, we calculated the ratio of RU21 to RU05 estimated fall velocities between the two gliders as well as the ratio of RU21 to RU05 depth-averaged glider velocities, which should be approximately equal to the ratio of friction velocities (Fig. 14). Fall velocity ratios were initially high, similar to RU21 fall velocities and grain-size. From 4:00 to 22:00 GMT on the 13th fall velocity ratios are near one. On the 14th the RU21 to RU05 fall velocity ratio increased by over a factor of two, until they drop again late on the 14th as the gliders began to turn onshore. The ratio of RU21 to RU05 depth-averaged glider velocities was just below one for the duration of the resuspension event on November 13th through the 14th. Calculated standard deviations

of RU21 to RU05 fall velocities and depth-averaged glider velocities are 0.62 and 0.08 respectively. The much larger standard deviation in the estimated fall velocity ratio shows that differences in grain size and subsequently fall velocity plays a larger role than current variability in the resuspension and transport dynamics during this storm event. Comparison of our fall velocity ratio to slopes of optical backscatter profiles in Figs. 8 and 9 for RU21 and RU05 respectively, show that profiles were Rouse-like throughout the water column for the 13th and 14th for RU05. These profiles are indicative of full water column resuspension of relatively smaller particles, which remained in suspension for the duration of the event. Optical backscatter profiles from RU21 were much more vertical than RU05 until mid-day on the 14th when resuspension peaked throughout the water column. Later on the 14th and into the 15th profiles of RU21 optical backscatter demonstrated a near bottom layer, which along with fall velocities indicates that larger particles were falling out of suspension or unable to make it into the upper portion of the water column. The differences in grain size and resuspension characteristics from the northern glider, RU21 and southern glider RU05 show that even during the largest storms local variability in bed characteristics can play a major role in modulating sediment resuspension and subsequently transport on the continental shelf. Our study demonstrates that during storms on the continental shelf, variability in bottom character also drives local variability in the magnitude and direction of sediment transport. Through glider spatial surveys of sediment transport and resuspension, we have shown that detailed spatial surveys and continually updated spatial maps similar to those produced by Goff et al. (2008) may be necessary to fully understand water-column sediment transport. These spatial surveys will not only support further understanding of observational data over shelf-wide spatial scales, but can also be used to quantitatively enhance realistic regional sediment resuspension and transport models.

5. Conclusion

Here we have demonstrated the importance of utilizing novel ocean observation technology, such as gliders and CODAR to resolve shelf-scale resuspension and transport during storms. A fleet of autonomous gliders not only provided information on sediment transport and resuspension over large spatial areas, but

also emphasized the importance of local variability in grain-size on estimates of shelf-wide sediment resuspension and transport, even in the largest storms. With little observed influence from tides, Langmuir cells or topography, the simple balance between turbulent shear stress and fall velocity, which varies with grain-size, played a major role in observed differences in sediment resuspension and transport along the mid-shelf. Future inclusion of glider fleets and CODAR networks along with traditional tripod and buoy instrumentation will allow for a more holistic view of sediment transport and resuspension along continental shelves, during storm events in particular, when shipboard measurements are not possible. These data will also aid in developing more robust regional models by feeding real data into predictive models as storms occur. In order to further understand the dynamics of sediment resuspension and transport on shelf-wide scales, the inclusion of acoustic and holographic sensors in addition to optical sensors on glider platforms will be necessary. This will help to accurately identify the nature of suspended particles when sediment bed information is lacking and will also provide more *in situ* information regarding the magnitude and direction of current profiles and transport during storm events.

Acknowledgments

Data used in this study was acquired by the Rutgers University Coastal Ocean Observation Lab (R.U.COOL) and NOAA. R.U.COOL is supported by ONR, NOAA, IOOS, NSF, DHS, DoD, NASA, NOPP and the State of New Jersey. Glider data for this study came from a deployment for the NSF Ocean Observing Initiative as part of a Cyber Infrastructure Implementing Organization testbedding activity. We would also like to thank Teledyne-Webb Research for graduate student support and continued technical support. The Mid-Atlantic Bight High Frequency Radar network is funded by IOOS. This work was supported by ONR MURI grant number N000140610739, NOAA MARCOOS grant numbers NA07NOS4730221 and NA01NOS4730014 and NSF OOI NSF OCE 10307201 1/1.

References

Agrawal, Y.C., 2005. The optical volume scattering function: temporal and vertical variability in the water column off the New Jersey coast. *Limnology and Oceanography* 50, 1787–1794.

Agrawal, Y.C., Pottsmith, H.C., 2000. Instruments for particle size and settling velocity observations in sediment transport. *Marine Geology* 168, 89–114.

Amato, 1994. Sand and Gravel Maps of the Atlantic Continental Shelf. In: Service, M.M. (Ed.), OCS Monograph MMS, p. 35.

Barrick, D.E., 1971a. Theory of HF and VHF propagation across the rough sea, 1, the effective surface impedance for a slightly rough highly conducting medium at grazing incidence. *Radio Science* 6, 517–526.

Barrick, D.E., 1971b. Theory of HF and VHF propagation across the rough sea, 2, application to HF and VHF propagation above the sea. *Radio Science* 6, 527–533.

Beardsley, R.C., Boicourt, W.C., 1981. On estuarine and continental-shelf circulation in the middle Atlantic Bight. In: Warren, B.A., Wunsch, C. (Eds.), *Evolution of Physical Oceanography*. MIT Press, Cambridge, MA, pp. 198–241.

Bigelow, H.B., 1933. Studies of the waters on the continental shelf, Cape Cod to Chesapeake Bay. I. The cycle of temperature. *Papers in Physical Oceanography and Meteorology* 2, 1–135.

Boss, E., Pegau, W.S., Lee, M., Twardowski, M., Shybanov, E., Korotaev, G., Baratange, F., 2004. Particulate backscattering ratio at LEO 15 and its use to study particle composition and distribution. *Journal of Geophysical Research* 109, C01014.

Cacchione, D.A., Thorne, P.D., Agrawal, Y., Nidziako, N.J., 2008. Time-averaged near-bed suspended sediment concentrations under waves and currents: comparison of measured and model estimates. *Continental Shelf Research* 28, 470–484.

Chang, G.C., Dickey, T.D., Williams III, A.J., 2001. Sediment resuspension over a continental shelf during Hurricanes Edouard and Hortense. *Journal of Geophysical Research* 106, 9517–9531.

Chapman, R.D., Graber, H.C., 1997. Validation of HF radar measurements. *Oceanography* 10, 76–79.

Chen, K., He, R., 2010. Numerical investigation of the Middle Atlantic Bight shelfbreak frontal circulation using a high-resolution ocean hindcast model. *Journal of Physical Oceanography* 40, 949–964.

Davis, R.E., Eriksen, C.E., Jones, C.P., 2003. Autonomous buoyancy driven underwater gliders. In: Griffiths, G. (Ed.), *Technology and applications of autonomous underwater vehicles*. Taylor & Francis, New York, pp. 37–58.

Dzwonkowski, B., Kohut, J.T., Yan, X.-H., 2009a. Seasonal differences in wind-driven across-shelf forcing and response relationships in the shelf surface layer of the central Mid-Atlantic Bight. *Journal of Geophysical Research* 114, C08018.

Dzwonkowski, B., Kohut, J.T., Yan, X.-H., 2009b. Sub-inertial characteristics of the surface flow field over the shelf of the central Mid-Atlantic Bight. *Continental Shelf Research* 29, 1873–1886.

Gargett, A., Wells, J., Tejada-Martinez, A.E., Grosch, C.E., 2004. Langmuir supercells: a mechanism for sediment resuspension and transport in shallow seas. *Science* 306, 1925–1928.

Glenn, S., Arnore, R., Bergmann, T., Bissett, W.P., Crowley, M., Cullen, J., Gryzmski, J., Haidvogel, D., Kohut, J., Moline, M., Oliver, M., Orrico, C., Sherrell, R., Song, T., Weidemann, A., Chant, R., Schofield, O., 2004. Biogeochemical impact of summertime coastal upwelling on the New Jersey shelf. *Journal of Geophysical Research* 109, C12S02.

Glenn, S., Clayton, J., Twardowski, M., Bowers, L., Kerfoot, J., Kohut, J., Webb, D., Schofield, O., 2008. Glider observations of sediment resuspension in a Middle Atlantic Bight Fall transition storm. *Limnology and Oceanography* 53, 2180–2196.

Glenn, S., Schofield, O., 2009. Growing a distributed ocean observatory: Our view from the COOLroom. *Oceanography* 22, 112–129.

Glenn, S.M., Grant, W.D., 1987. A suspended sediment stratification correction for combined wave and current flows. *Journal of Geophysical Research* 92, 8244–8264.

Goff, J.A., Jenkins, C.J., Jeffress Williams, S., 2008. Seabed mapping and characterization of sediment variability using the usSEABED data base. *Continental Shelf Research* 28, 614–633.

Gong, D., Kohut, J.T., Glenn, S.M., 2010. Seasonal climatology of wind-driven circulation on the New Jersey shelf. *Journal of Geophysical Research* 115, C04006.

Grant, W.D., Madsen, O.S., 1979. Combined wave and current interaction with a rough bottom. *Journal of Geophysical Research* 84, 1797–1808.

Grant, W.D., Madsen, O.S., 1986. The continental-shelf bottom boundary layer. *Annual Review of Fluid Mechanics* 18, 265–305.

Harcourt, R.R., D'Asaro, E.A., 2010. Measurement of vertical kinetic energy and vertical velocity skewness in oceanic boundary layers by imperfectly Lagrangian floats. *Journal of Atmospheric Oceanic Technology* 27, 1918–1935 <<http://dx.doi.org/proxy.libraries.rutgers.edu/10.1175/2010JTECH0731.1>>.

Harris, C.K., Butman, B., Traykovski, P., 2003. Winter-time circulation and sediment transport in the Hudson Shelf Valley. *Continental Shelf Research* 23, 801–820.

Houghton, R.W., Schlitz, R., Beardsley, R.C., Butman, B., Chamberlin, J.L., 1982. The Middle Atlantic Bight cold pool: evolution of the temperature structure during summer 1979. *Journal of Physical Oceanography* 12, 1019–1029.

Keen, T.R., Glenn, S.M., 1995. A coupled hydrodynamic-bottom boundary layer model of storm and tidal flow in the Middle Atlantic Bight of North America. *Journal of Physical Oceanography* 25, 391–406.

Kohut, J.T., Roarty, H.J., Glenn, S.M., 2006. Characterizing observed environmental variability With HF Doppler Radar Surface Current Mappers and Acoustic Doppler Current Profilers: environmental variability in the coastal ocean. *IEEE Journal of Oceanic Engineering* 31, 876–884.

Lentz, S., Guza, R.T., Elgar, S., Feddersen, F., Herbers, T.H.C., 1999. Momentum balances on the North Carolina inner shelf. *Journal of Geophysical Research* 104, 18205–18226.

Lentz, S.J., 2003. A climatology of salty intrusions over the continental shelf from Georges Bank to Cape Hatteras. *Journal of Geophysical Research* 108, 3326.

Lentz, S.J., 2008. Seasonal variations in the circulation over the Middle Atlantic Bight continental shelf. *Journal of Physical Oceanography* 38, 1486–1500.

McBride, R.A., Moslow, T.F., 1991. Origin, evolution, and distribution of shoreface sand ridges, Atlantic inner shelf, U.S.A. *Marine Geology* 97, 57–85.

Ohlmann, C., White, P., Washburn, L., Terrill, E., Emery, B., Otero, M., 2007. Interpretation of coastal HF Radar-derived surface currents with high-resolution drifter data. *Journal of Atmospheric & Oceanic Technology* 24, 666–680.

Reid, J.M., Reid, J.A., Jenkins, C.J., Hastings, M.E., Williams, S.J., Poppe, L.J., 2005. usSEABED: Atlantic coast offshore surficial sediment data release. U.S. Geological Survey Data Series, 1st ed.

Roarty, H., Glenn, S., Kohut, J., 2010. Operation and application of a regional high-frequency radar network in the Mid-Atlantic Bight. *Marine Technology Society Journal* 44, 133–145.

Roesler, C.S., Boss, E., 2008. In situ measurement of the inherent optical properties (IOPs) and potential for harmful algal bloom (HAB) detection and coastal ecosystem observations, Chapter 5. In: Babin, M., Roesler, C.S., Cullen, J. (Eds.), *Real-Time Coastal Observing Systems for Marine Ecosystem Dynamics and Harmful Algal Blooms: Theory, Instrumentation and Modeling*; UNESCO, pp. 153–206.

Schofield, O., Glenn, S., Orcutt, J., Arrott, M., Meisinger, M., Gangopadhyay, A., Brown, W., Signell, R., Moline, M., Chao, Y., Chien, S., Thompson, D., Balasuriya, A., Lermusiaux, P., Oliver, M., 2010a. Automated sensor network to advance ocean science. *Eos Transactions, American Geophysical Union* 91 (39), 345–356.

- Schofield, O., Kohut, J., Aragon, D., Creed, L., Graver, J., Haldeman, C., Kerfoot, J., Roarty, H., Jones, C., Webb, D., Glenn, S., 2007. Slocum gliders: robust and ready. *Journal of Field Robotics* 24, 473–485.
- Schofield, O., Kohut, J., Glenn, S., Morell, J., Capella, J., Corredor, J., Orcutt, J., Arrott, M., Krueger, I., Meisinger, M., Peach, C., Vernon, F., Chave, A., Chao, Y., Chien, S., Thompson, D., Brown, W., Oliver, M., Boicourt, W., 2010b. A regional slocum glider network in the Mid-Atlantic Bight leverages broad community engagement. *Marine Technology Society Journal* 44, 185–195.
- Stewart, R.H., Joy, J.W., 1974. HF radio measurements of surface currents. *Deep Sea Research and Oceanographic Abstracts* 21, 1039–1049.
- Styles, R., Glenn, S.M., 2000. Modeling stratified wave-current bottom boundary layers for the continental shelf. *Journal of Geophysical Research* 105, 24119–24139.
- Styles, R., Glenn, S.M., 2002. Modeling bottom roughness in the presence of wave-generated ripples. *Journal of Geophysical Research* 107, 3110.
- Styles, R., Glenn, S.M., 2005. Long-term sediment mobilization at a sandy inner shelf site, LEO-15. *Journal of Geophysical Research* 110, C04S90.
- Swift, D.J.P., Field, M.E., 1981. Evolution of a classic sand ridge field: Maryland sector, North American inner shelf. *Sedimentology* 28, 461–482.
- Teague, C.C., 1971. *High Frequency Resonant Scattering Techniques for the Observation of Directional Ocean-Wave Spectra*, Calif. Stanford University, Palo Alto.
- Terrill, E.J., Melville, W.K., Stramski, D., 2001. Bubble entrainment by breaking waves and their influence on optical scattering in the upper ocean. *Journal of Geophysical Research* 106, 16815–16823.
- Traykovski, P., 2007. Observations of wave orbital scale ripples and a nonequilibrium time-dependent model. *Journal of Geophysical Research* 112, C06026.
- Traykovski, P., Hay, A.E., Irish, J.D., Lynch, J.F., 1999. Geometry, migration, and evolution of wave orbital ripples at LEO-15. *Journal of Geophysical Research* 104, 1505–1524.
- Twardowski, M.S., Boss, E., Macdonald, J.B., Pegau, W.S., Barnard, A.H., Zaneveld, J.R.V., 2001. A model for estimating bulk refractive index from the optical backscattering ratio and the implications for understanding particle composition in case I and case II waters. *Journal of Geophysical Research* 106, 14129–14142.
- Wiggert, J.D., Jones, B.H., Dickey, T.D., Brink, K.H., Weller, R.A., Marra, J., Codispoti, L.A., 2000. The Northeast monsoon's impact on mixing, phytoplankton biomass and nutrient cycling in the Arabian Sea. *Deep Sea Research Part II: Topical Studies in Oceanography* 47, 1353–1385.
- Xu, Y., Chant, R., Gong, D., Castelao, R., Glenn, S., Schofield, O., 2011. Seasonal variability of chlorophyll a in the Mid-Atlantic Bight. *Continental Shelf Research* 31, 1640–1650.
- Zedler, S.E., Dickey, T.D., Doney, S.C., Price, J.F., Yu, X., Mellor, G.L., 2002. Analyses and simulations of the upper ocean's response to Hurricane Felix at the Bermuda Testbed Mooring site 13–23 August 1995. *Journal of Geophysical Research* 107, 3232.